Current Journal of Applied Science and Technology

41(29): 37-52, 2022; Article no.CJAST.85067

ISSN: 2457-1024

(Past name: British Journal of Applied Science & Technology, Past ISSN: 2231-0843, NLM ID: 101664541)

Density Current Simulations In Cold Fresh Water And Its Cabbeling phenomenon: A Comparative Analysis With Given Experimental Results

Alabodite Meipre George [a*] **and Evans Fiebibiseighe Osaisai** [a]

[a] *Department of Maths/Computer Science, Niger Delta University, Wilberforce Island, Bayelsa State, Nigeria.*

Authors' contributions

This work was carried out in collaboration between both the authors. Both authors have read and approved the final manuscript.

Article Information

DOI: 10.9734/CJAST/2022/v41i2931801

Open Peer Review History:
This journal follows the Advanced Open Peer Review policy. Identity of the Reviewers, Editor(s) and additional Reviewers, peer review comments, different versions of the manuscript, comments of the editors, etc are available here: https://www.sdiarticle5.com/review-history/85067

Original Research Article

Received 22 May 2022
Accepted 28 July 2022
Published 17 August 2022

ABSTRACT

The behaviour of warm water discharge at a temperature T_m horizontally into a homogeneous body of cold fresh water at a temperature $T = 0$ was investigated by means of a numerical model through lock-exchange. Water density here was taken to be a quadratic function of temperature. This work as presented here is practical and relevant to many fields of study and also enhances policy making towards the protection of the aquatic ecosystems. Such scenarios are evident in lakes, especially in holomictic lakes and warm discharge from thermoelectric power generating plants. Because the sudden increase in the water temperature after discharge will leads to "thermal shock" killing aquatic life that has become acclimatised to living in a stable temperate environment. The aim of this investigation is to better fathom and as well, gain more insight into such studies. Cabbeling process was key as whenever fluid of different temperature come in contact and as well as the development of Kelvin-Helmholtz instability in the interaction surface. The general behaviours here are dependent of lock volume, density difference and Reynolds number. We noticed that the collapsing velocity of the denser fluid within the first time frame was high, higher than every fluid movement elsewhere. Relations that describes the various regimes of flow were also drawn, and as well as those for the spreading distance L_{dc} of the density current. However, there are little variations in the scaling laws as compared to the earlier studied cases where density difference was by the means of salt water. But for those where density difference is as a result of temperature,

**Corresponding author: E-mail: georgianalgebra@gmail.com;*

we believe that these results are a good starting point to better fathom and as well, gain more insight into such studies. Lastly, the consideration of barrier position is key, being that the lock volume is also believed to be a factor. Researchers can also gain more knowledge in terms of the dynamics of such flows.

Keywords: Kurtosis; T-test; wilcoxon signed-rank test; normal distribution; uniform distribution; T-distribution; laplace distribution.

1 INTRODUCTION

Density currents are a phenomenal behaviours that occur in many practical applications both in nature and man-made situations, and examples of such scenarios are given in [1, 2, 3, 4] . These currents (flows) are mainly driven by difference in density between the flow fluid and the ambient fluid. Considering the river systems, such flows are evident because part of the water in some river mouth, lakes, etc., is saltier or colder and in turn will form density current. In some cases, the water in such areas also contains more suspended sediment than the surrounding water. Thus, these currents are also known to be responsible for the transportation of sediments in reservoirs [5].

Researchers have also extensively studied these behaviours experimentally, theoretically and numeri-cally and have given some mathematical relations and values that describes the propagation speed and spreading distance of such currents and as well as identifying different regimes of flow [2, 6, 7]. However, earlier works on density currents can be found in [8, 9, 10]. Where a much simplified theoretical model that describes the evolution of the frontal head after the release of a denser fluid into a lighter ambient fluid was suggested. A derivation of theoretical model for the initiation of a steady two-dimensional density current in a rectangular channel, and numerical solutions by using the shallow-water equation for a two-layer fluid that has to do with an empirical front condition were also obtained. However, in most of the configurations, the lock-exchange method is used Fig. 1: as this enables such flow scenarios over the rough and smooth horizontal surfaces and as well as the inclined surfaces. In such experimental cases, salt is mostly used to create the density difference in fresh water. Example of such studies with this lock-exchange configuration with saltwater and fresh water include [6, 7, 11, 12 - 15, 25].

More so, it is also known that when water masses on either side of the temperature of maximum density (T_m) come in contact, cabbeling is likely to occur even as the various fluids advance in their opposite directions. It is believed that the denser fluid will penetrate the ambient fluid on the floor and form a density current. Such scenarios are also evident in lakes, especially in holomictic lakes and warm discharge from thermoelectric power generating plants. We can see [2, 7, 16, 17] for more insights and a more detailed literature review in other to minimise repetition. However, density currents flows through lock-exchange whereby density variation is as a result of temperature difference had not received much attention as compared to that with saltwater that is widely used [6].

Generally, gravity currents usually undergo either two or three distinct phases of flow and these include: a slumping phase, self-similar phase and viscous phase. As also recorded by [18], after the instantaneous removal of the gate, an initial adjustment phase where the advancing head varies with approximately constant velocity. Followed immediately by the second phase after the ambient fluid had reflected at the rear wall, it in turn overtakes the penetrating head of the current. If only the lock-exchange experiment was carried out in a finite confined channel [10]. At this point in the flow, the penetrating head advances as $t^{2/3}$, but decreases with front speed as $t^{-1/3}$, where t is the time after which the gate was removed. Lastly, is the phase where viscous effects overcome inertial effects and the current front velocity decreases more rapidly as $t^{-4/5}$, with front position advancing as $t^{1/5}$ [19].

Recently, we have also considered a "Numerical Simulations of the Cabbeling phenomenon in Surface Gravity Currents in Cold Fresh Water"

where we have extensively discussed the behaviour of such flows taken density as a quadratic function of temperature. Relations were also drawn that describes the propagation speed of the frontal head and as well as the distance traveled with respect to time [2]. The behaviour of the negatively buoyant plume as mixed fluid that have mixed up to the T_m was also key. But then, behaviour of the descended fluid on the floor was not fully captured and as such, the propagation speed of the density current was not detailed. Though, this might be as a result of the limited domain space used for the computation.

These authors [20, 21] in their works have also considered density current through lock-exchange, where density variation was as a result of temperature difference. But then, they have not really presented a detailed description of the evolution of the frontal head and as well as obtaining some empirical scaling laws that will describe the propagation speed and spread length of the density current. We have considered this to be very important because there is need for comparison with previous results for more insights. For this reason, we have decided to carryout this investigation so as to better fathom and as well, gain more insight into such studies. Thus, taken into consideration here is the motion of fluids with T_m (which is $3.98^{\circ}C$ for fresh water at atmospheric pressure, (i.e., approximately $4^{\circ}C$ in some numerical calculation)) initially at rest but separated by a vertical barrier in a rectangular domain with an ambient fluid with temperature zero. It is expected that difference in the hydrostatic pressure will result in the denser fluid flowing in one direction along the floor once the barrier is lifted up. Meanwhile the less dense fluid will flow in the opposite direction horizontally along the upper part of the domain, and this in turn create a mixing layer between the two fluids as they interact with each other. However, the interaction process will continue even as the most dense fluid is located at the lower part with a frontal or leading head penetrating the ambient fluid. This will continue until the dense but warm fluid will mix to a point where both fluids attain the same temperature.

Our present investigation is based on numerical simulations that uses the lock exchange method with the assumption that density is a quadratic function of temperature. Density current which contains a dense but warm fluid in this case is expected to mix further as it spreads outward on the floor. This will continue until the dense fluid will mix to a point where it attain the same temperature with the ambient fluid. Though, this will be feasible if the domain of computation is extremely large or infinite.

We will vary computational domain between length $L = 7000$, i.e., $0 \leq X \leq 7000$, with a domain height $H = 1000$ i.e., $0 \leq Y \leq 1000$ in the first instance with barrier position $L/14$. And a computational domain length $L = 10000$, i.e., $0 \leq X \leq 10000$, with a domain height $H = 1200$ i.e., $0 \leq Y \leq 1200$ in the second instance with barrier position $0.07L/14$. The input fluid temperature in both cases is $\phi_{in} = 1$ on the right hand side. Meanwhile, on the left hand side, at position $13L/14$ and $13.93L/14$, $\phi_{in} = 0$. Where L is the total length of the computational domain and ϕ_{in}, the initial temperature on the various sides of the barrier. Now, reason for the various computational domain is to enable us capture important features and processes for detailed analysis.

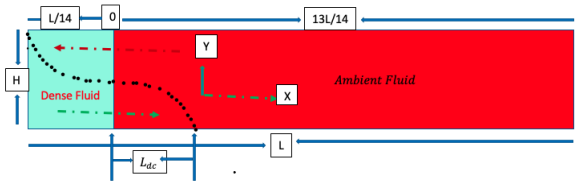

Fig. 1. Schematic presentation of Lock-exchange flow in a channel of length L and height H. The dotted line gives the interface between the two fluids some time after the release

2 MODEL FORMULATION AND GOVERNING EQUATIONS

The behaviour of density currents as denser fluid spread outwards on the floor after the lock release due to the nonlinear relation between density ρ and temperature T is very paramount. Thus, the relation below is useful for this study,

$$\rho = \rho_m - \beta(T - T_m)^2 \tag{2.1}$$

This, we believe gives a very good fit to the experimentally determined density of fresh water at temperature below $10^{\circ}C$ if we consider T_m = $3.98^{\circ}C$, ρ_m = 1.000×10^3 $kg.m^{-3}$ and β = 8.0×10^{-3} $kg.m^{-3}(^{\circ}C)^{-2}$ [22, 23] and all other fluid properties (e.g. viscosity, thermal diffusivity) are assumed constant. We also assume that the flow is time dependent and two dimensional, and that the liquid property is constant except for the water density, which changes with temperature and in turn results to the buoyancy force. We can non-dimensionalise the coordinates x, y, velocity components u, v, time t, pressure p and temperature T by

$$U = \frac{u}{U_*} \quad V = \frac{v}{U_*} \quad X = \frac{x}{H} \quad Y = \frac{y}{H} \quad \tau = \frac{t}{\frac{H}{U_*}} \quad P = \frac{p}{\rho U_*^2}$$

$$\phi = \frac{T - T_\infty}{T_m - T_\infty}, \tag{2.2}$$

where x and u are horizontal, y and v are vertical; $U_* = \sqrt{\frac{\rho_\infty - \rho)}{\rho} H}$ is the relative frontal velocity and domain height H. We also define dimensionless parameters, the Reynolds Re, Prandtl Pr and Froude Fr numbers, by:

$$\nu = \frac{\mu}{\rho} \quad \alpha = \frac{k}{\rho c_p} \quad Re = \frac{U_* H}{\nu} \quad Pr = \frac{\nu}{\alpha} \quad Fr^2 = \frac{\rho_m U_*^2}{g\beta(T_m - T_\infty)^2 H}, \tag{2.3}$$

where ν and α are the respective diffusivities of momentum and heat, and μ is viscosity, k is thermal conductivity and c_p is specific heat capacity. In terms of these dimensionless variables and parameters, the continuity equation, the horizontal and vertical momentum equations and the thermal energy equation are given as

$$\frac{\partial U}{\partial X} + \frac{\partial V}{\partial Y} = 0 \tag{2.4}$$

$$\frac{\partial U}{\partial \tau} + U\frac{\partial U}{\partial X} + V\frac{\partial U}{\partial Y} = -\frac{\partial P}{\partial X} + \frac{1}{Re}\left(\frac{\partial^2 U}{\partial X^2} + \frac{\partial^2 U}{\partial Y^2}\right) \tag{2.5}$$

$$\frac{\partial V}{\partial \tau} + U\frac{\partial V}{\partial X} + V\frac{\partial V}{\partial Y} = -\frac{\partial P}{\partial Y} + \frac{1}{Re}\left(\frac{\partial^2 V}{\partial X^2} + \frac{\partial^2 V}{\partial Y^2}\right) + \frac{1}{Fr^2}[\phi^2 - 2\phi] \tag{2.6}$$

$$\frac{\partial \phi}{\partial \tau} + U\frac{\partial \phi}{\partial X} + V\frac{\partial \phi}{\partial Y} = \frac{1}{RePr}\left(\frac{\partial^2 \phi}{\partial X^2} + \frac{\partial^2 \phi}{\partial Y^2}\right) \tag{2.7}$$

The terms U_{dc} and L_{dc} are used to describe the propagating speed and spread length of the density current.
Our initial conditions are an undisturbed, homogeneous medium as also given in [2].

$$U = 0, \quad V = 0, \quad \phi = 0, \quad for \quad \tau < 0 \tag{2.8}$$

For $\tau \geq 0$ we have boundary conditions as follows. On the side walls:

$$U = 0, \quad V = 0, \quad \frac{\partial \phi}{\partial X} = 0 \tag{2.9}$$

At the plume source:

$$U = U_*, \quad V = 0, \quad \phi_{in} = 1 \text{ for } L/14 \text{ and } 0.07L/14 \text{ and } \phi_{in} = 0 \text{ for } 13L/14 \text{ and } 13.93L/14, \quad \text{for} \quad X = 0, \, at \, Y = H \quad (2.10)$$

On the floor of the domain:

$$U = 0, \quad V = 0, \quad \frac{\partial \phi}{\partial Y} = 0 \quad (2.11)$$

At the top of the domain:

$$\frac{\partial U}{\partial Y} = 0, \quad V = 0, \quad \frac{\partial \phi}{\partial Y} = 0 \quad (2.12)$$

The Reynolds number $Re = 50$, Froude number $Fr = 1$ and Prandtl number $Pr = 11$ will be fixed throughout this investigation. The dimensionless temperature $\phi_{in} = 1$ on $L/14$ and $0.07L/14$ is equivalent to a discharge at $4^{\circ}C$ into an ambient at $0^{\circ}C$. Numerical solution of the above equations is by means of COMSOL Multiphysics software. This commercial package uses a finite element solver with discretization by the Galerkin method and stabilisation to prevent spurious oscillations. We have used the "Extremely fine" setting for the mesh. Time stepping is by COMSOL's Backward Differentiation Formulas. Further information about the numerical methods is available from the COMSOL Multiphysics website [24]. Results will be illustrated mainly by surface temperature plots of dimensionless temperature on a colour scale from dark red for the ambient temperature $\phi = 0.0$, through yellow to white for the source temperature $\phi = 1$. Except at some point in the density current where we may have repeated temperature colour scale for a different temperature. Note that $\phi = 1.0$ corresponds to the temperature of maximum density.

3 RESULTS

The results below show the behaviour of warm but dense fluid, discharged at $4^{\circ}C$ through lock-exchange in cold fresh water. Reynolds number $Re = 50$, Froude number $Fr = 1$ and Prandtl number $Pr = 11$, are kept fixed throughout the study. Computational domain were also varied between $L = 7000$ and $L = 10000$ with barrier position between $L/14$ and $0.07L/14$ respectively. Fig. $2, 3, 4, 5, 6, 7, 8 \,\&\, 9$ show the evolution of temperature field for $\phi_{in} = 1$ within the time range $0 \leq \tau \leq 425$ and $0 \leq \tau \leq 1800$ in the various cases for a thorough analysis. Barrier position in the case as shown in Fig. 2 is at $L/14$, with $\phi_{in} = 1$ on the right hand side, and $\phi_{in} = 0$ on the left hand side. Meanwhile, the case as shown in Fig. 4 is at $0.07L/14$, with $\phi_{in} = 1$ on the right hand side, and $\phi_{in} = 0$ on the left hand side.

A collapsing behaviour of the warm but denser fluid was observed within the first few time interval of the simulation, immediately after the removal of the barrier vertically upwards. A cabbeling process also begins within the same time at the point where the water masses meet, even as the denser fluid on the right hand side began to form density current (see Fig. 2(b) & 4(b)). A significant mixed fluid was not observed within this period and this might be as a result of the fact that the temperature difference between the two fluid is small. However, as time progresses, we observed the development of Kelvin-Helmholtz instabilities at the interaction layer between the ambient and the denser fluid. This unstable structures ranges from the penetrating head to the rear of the density current (see Fig. 2(c - e)); though, this is not obvious in Fig. 4(c - e) because of its reduced volume. However, the most dense fluid continue to penetrate the ambient fluid with a sharp frontal head.

Figs. 4(d) - (e) show a very different behaviour as compared to those in Figure 2(d) - (e). We observed in the former that the collapsing velocity of the denser fluid was high, higher than every fluid movement elsewhere. Thus, on getting the floor of the domain there was an intense

(vigorous) mixing which had led to a major depletion in its temperature and this is evident afterwards as compared to the later (see Fig. 3(f) - (g) & 5(f) - (g)). This in turn resulted in a rapidly reduced motion because the dense but warm fluid is no longer energetic enough to advance quickly Fig. 5(f) - (g). However, the frontal motion of the head of this density current continue to spread further, penetrating the ambient fluid and maintaining the unstable layer even as this (Kelvin-Helmholtz instabilities) increases with time (see Fig. 3(h) - (j), Fig. 6 and Fig. 7). As the denser fluid advances, it was also observed that the frontal head is always found to be replenished by a ground flow of warm but dense unadulterated water from the rear, enabling the density current to push further (see Fig. 3(i) - (j)). Whereas, Figs. 6, 7, 8 & 9 still contains some mildly warm fluid at the rear. This is as a result of the initial intense mixing after the lock release that have resulted in the denser fluid not being energetic to penetrate further. Thus, it takes much longer time to advance to the position of the frontal head.

During the flow, the motion of the density current decreases in a stepwise manner even as the Kelvin-Helmholtz instabilities dies out at the rear (see Fig. 3(i) - (j) & Fig. 9). The possible explanation to this behaviour might be as a result of the regrouping process after the raging columns of the Kelvin-Helmholtz instabilities had separated/partitioned the denser fluid. This process will continue until the denser fluid will attain the same temperature with the ambient fluid (see Fig. 3(h) - (j)). This is also the primary cause why the slightly warm fluid in Figure 6, 7, 8 & 9 is seen at the rear though, not energetic. The volume of dense but warm fluid reduces significantly as time progresses after the density current had moved a remarkable distance L_{dc} and as well as the propagation speed U_{dc} (almost to a halting state in this case with barrier position $0.07L/14$): and U_{dcc} (still energetic to penetrate further) as compared to the former, when measured from the barrier position. The density current will eventually halt as this attain the same temperature with the ambient fluid Fig. 9.

With these information provided, we can clearly state that three phases or regimes of flow exist. First was the collapsing phase. This occur after the removal of the barrier, where water rapidly reorganised itself on the floor to advance forward. The second was a phase of rapid depletion of temperature. And this was as a result of the intense mixing after the collapsing phase, which resulted in a very slow motion. The temperature of the denser fluid at this point had reduced drastically, so was not energetic enough to accelerate faster. The third phase is the stepwise movement phase. This was the phase we observed much of the Kelvin-Helmholtz instabilities at the interaction layer. Where partitions were created from the raging columns of the Kelvin-Helmholtz instabilities in the denser fluid.

We can now comfortably state that the various behaviours as observed here in this paper also correspond to some of the earlier experimentally studied cases by [6, 11, 19, 20, 25, 26]. That the instantaneous release of the two fluids after gate was removed led to an initial adjustment phase where the advancing head varies with approximately constant velocity. However, we have also highlighted a speedy collapsing behaviour in the denser fluid within this time frame. Such that its movement is higher than every other fluid movement elsewhere. This behaviour is evident in Fig. 12(a) where there is a rapid linear movement. It has also been recorded that the second phase begins immediately after the ambient fluid had reflected at the rear wall, which in turn overtakes the penetrating head of the density current. In this phase our result showed a rapid depletion of temperature which might be as a result of the intense mixing after the denser fluid landed. This also resulted in a very slow fluid motion being that the temperature of the denser fluid at this point had reduced drastically, so was not energetic enough to accelerate faster.

The third phase is the phase where viscous effects overcome inertial effects and the current front velocity decreases more rapidly as $t^{-\frac{4}{5}}$ as also cited in [2]. In this present study, our result show a stepwise movement. This was the phase we observed much of the Kelvin-Helmholtz instabilities at the interaction layer that was responsible for the partitions in the denser fluid. The overall behaviour as observed here in this investigation might be as a result of the

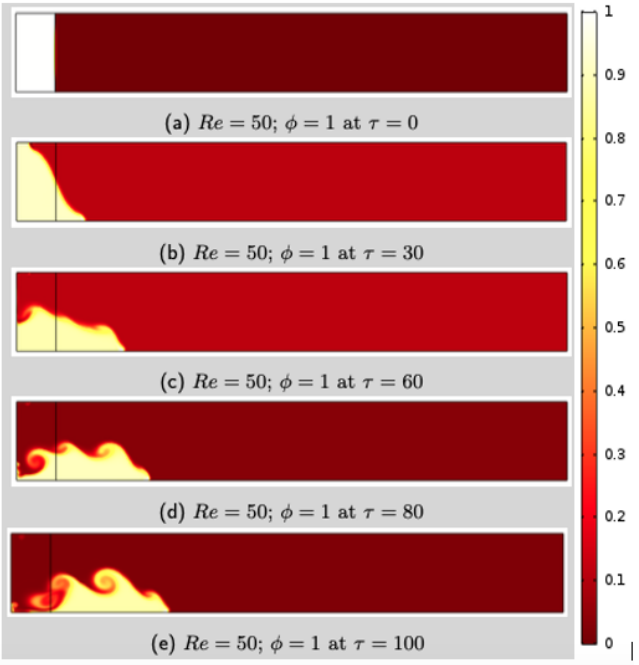

Fig. 2. Evolution of temperature field in the Density current for $Fr = 1$ and Reynolds number $Re = 50$ with $\phi = 1$ at time $0 \leq \tau \leq 100$

small volume of dense fluid used. Because this requires a very little mixing before it attain the same density with the ambient fluid. Thus, during the collapsing (slumping) phase most of the fluid had attained $\phi_{in} = 0$. The strong interaction between the ambient fluid because of its height and the dense fluid also contributed to the slow movement of the current as time progresses. Even though the choice of numerical parameters (Reynolds number 50) for a laminar flow was suggested and ideal for the purpose of this work [6, 11, 25]. It is worth emphasising that in most of the lock-exchange experimental cases, salt is mostly used to create the density difference. Except for Bukreev [20, 21] who considered density variation as a result of temperature difference, but did not really give much details.

Profiles of temperature and horizontal velocity component on the density current at the height $Y = 100$, some distance above the floor were also examined. This enables us to gain more information on the spreading behaviour of the density current for effective analysis as shown in Figure10 and Figure.11. Profiles of temperature as shown in Fig.10 indicate that there was a serious depletion of temperature within the first few interval between $L = 0 - 200$, except at $\tau = 30$ where there was still some fairly warm fluid within the range. At time $\tau = 60$, within the interval $L = 200 - 600$, we could trace fairly undiluted denser fluid. This we also believed to be true because the development of Kelvin-Helmholtz instabilities is yet to begin at that point in time. Thereafter, there was intense mixing also resulting from the Kelvin-Helmholtz instabilities leading to further depletion of temperature downstream. Most of the fluid within the time range $500 \leq \tau \leq 1800$ at that level was already at the same temperature with the ambient fluid. Thus, we can conclude that, temperature decreases rapidly with time at that level. Fluctuations in the temperature profiles also confirm that decrease in temperature with horizontal length is not monotonic. In like manner, profiles of horizontal velocity as shown in (Fig.11) indicate that there was some level

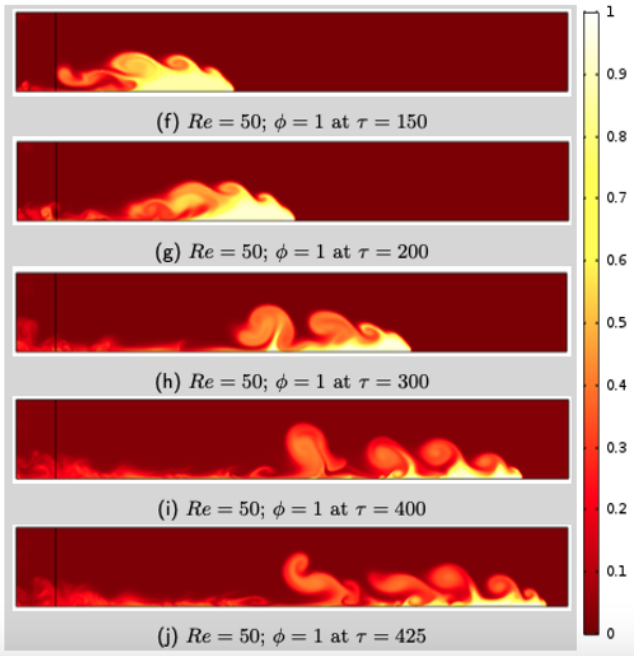

Fig. 3. Evolution of temperature field in the Density current for $Fr = 1$ and Reynolds number $Re = 50$ with $\phi = 1$ at time $150 \leq \tau \leq 425$

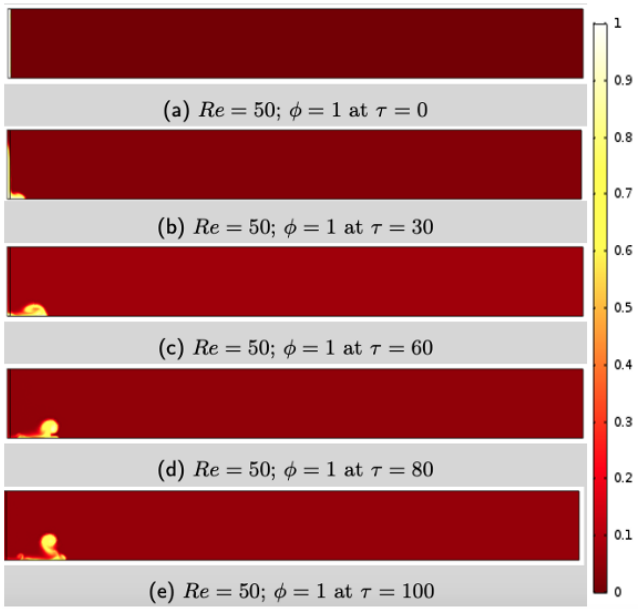

Fig. 4. Evolution of temperature field in the Density current for $Fr = 1$, $Pr = 11$ and $Re = 50$ with $\phi = 1$ at time $0 \leq \tau \leq 100$

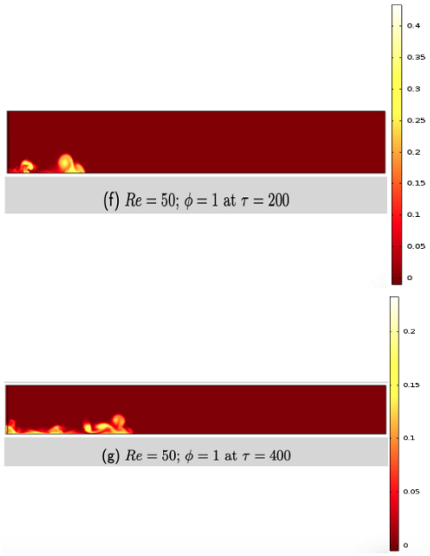

Fig. 5. Evolution of temperature field in the Density current for $Fr = 1$, $Pr = 11$ and $Re = 50$ with $\phi = 1$ at time $200 \leq \tau \leq 400$

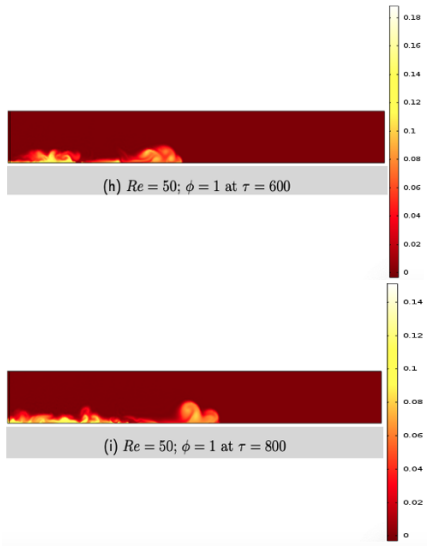

Fig. 6. Evolution of temperature field in the Density current for $Fr = 1$, $Pr = 11$ and $Re = 50$ with $\phi = 1$ at time $600 \leq \tau \leq 800$

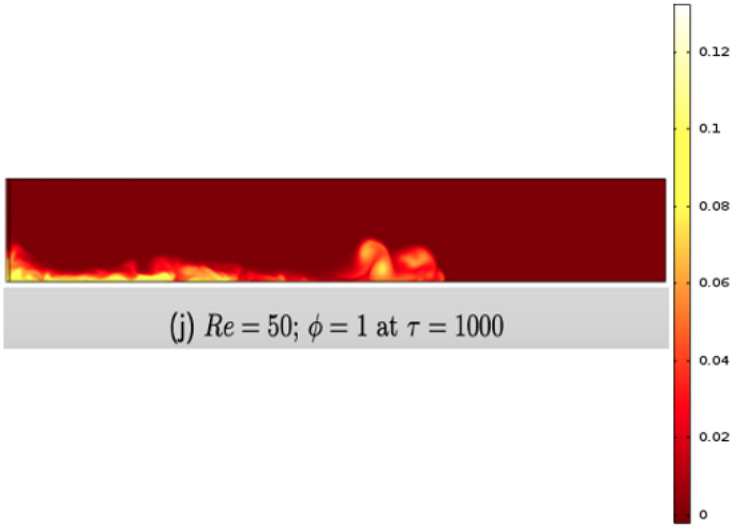

Fig. 7. Evolution of temperature field in the Density current for $Fr = 1$, $Pr = 11$ and $Re = 50$ with $\phi = 1$ at time 1000

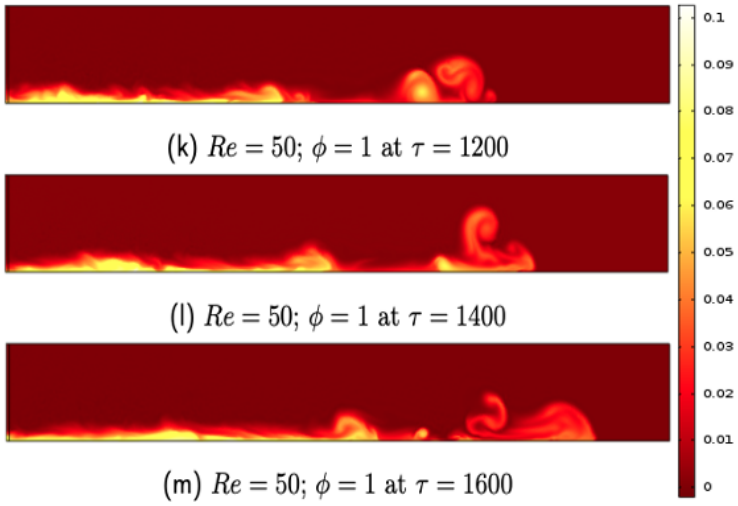

Fig. 8. Evolution of temperature field in the Density current for $Fr = 1$, $Pr = 11$ and $Re = 50$ with $\phi = 1$ at time $1200 \leq \tau \leq 1600$

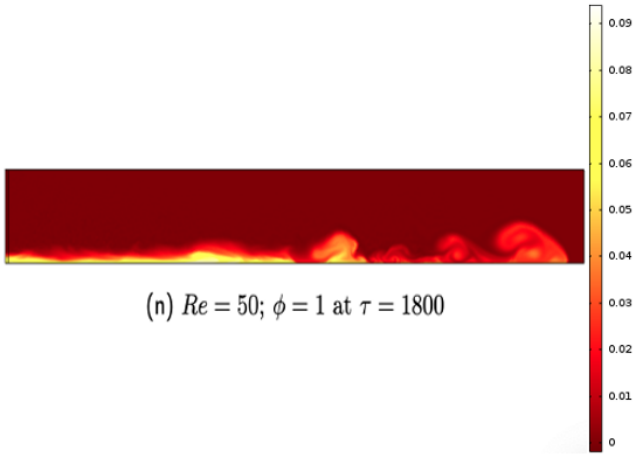

(n) $Re = 50;\ \phi = 1$ at $\tau = 1800$

Fig. 9. Evolution of temperature field in the Density current for $Fr = 1$, $Pr = 11$ and $Re = 50$ with $\phi = 1$ at time 1800

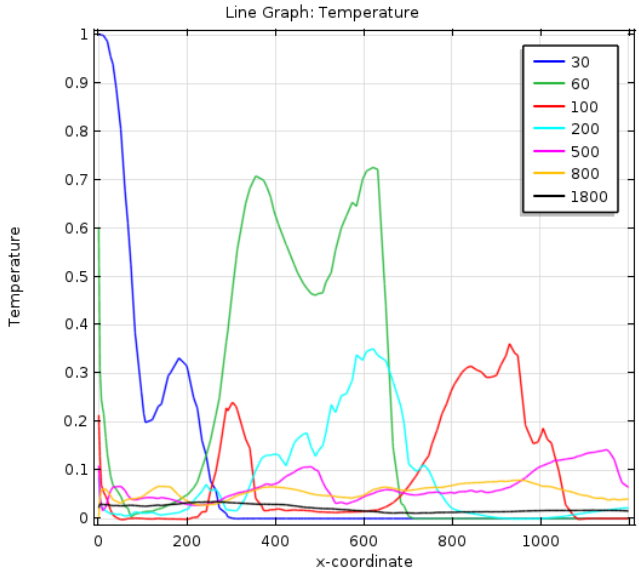

a)$Re = 50;\ \phi = 1$ and $Pr = 11$

Fig. 10. Dimensionless temperature profiles at some point close to the floor of the domain $\phi(X, 100)$ at time $\tau = 30, 60, 100, 200, 500, 800, 1800$ in the Density current for $Re = 50$, $Pr = 11$, $\phi_{in} = 1$ and $Fr = 1$

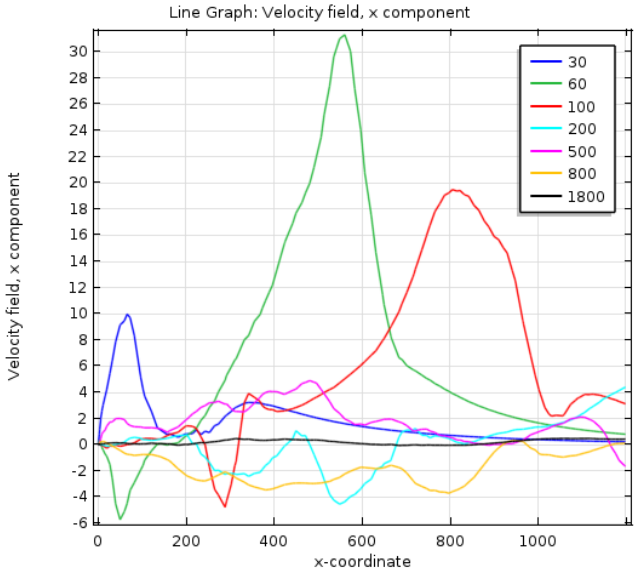

a)$Re = 50$; $\phi = 1$ and $Pr = 11$

Fig. 11. Dimensionless horizontal velocity profiles at some point close to the surface $V(X, 100)$ **at time** $\tau = 30, 60, 100, 200, 500, 800, 1800$ **in the Density current for** $Re = 50$**,** $Pr = 11$**,** $\phi_{in} = 1$ **and** $Fr = 1$

of backward and forward movement of fluid at that level. The possible explanation to this might be as a result of the interaction layer between the two fluid, where Kelvin-Helmholtz instabilities was observed. As the frontal head pushes forward, the mixed fluid that is up to $\phi = 0$ move backwards with the aid of the Kelvin-Helmholtz instabilities. Though, a very fast forward movement of the fluid was also evident at some point $X = 500\, and\, 800$. It is worth indicating that both profiles of temperature and that of velocity are determined from the simulation as shown in Fig. 9.

The propagation speed with which the frontal head of the density current U_{dc} travels with time τ_n is also presented and shown with a linear and logarithmic scale in Figure 12(a) for simulations with barrier point $0.07L/14$. As described earlier, the results here had shown three phases or regimes of flow. First was the collapsing phase which correspond to the description as given in [6, 11, 20] (slumping phase). This occurs after the removal of the barrier, where water rapidly reorganised itself on the floor to advance forward. However, we have recorded the case that the collapsing velocity of the denser fluid within this time frame is high, higher than every fluid movement elsewhere. This behaviour is evident in Fig. 12(b) where there is a rapid linear movement. Therefore, we can identify a single regime in this phase of flow from an empirically determined data set, and this is shown as a straight line that represents the best fit power laws obtained by linear regression of $logU_{dc1}$ on $log\tau_n$:

$$U_{dc1} = 1.071\tau_n^{0.9511} \quad [R^2 = 0.9994] \qquad (3.1)$$

where R^2 is the regression coefficient in each case.

Second was the phase of rapid depletion of temperature because of the intense mixing during the reorganising process on the floor. This we can liken to as the self-similar phase where after the ambient fluid had reflected at the rear wall

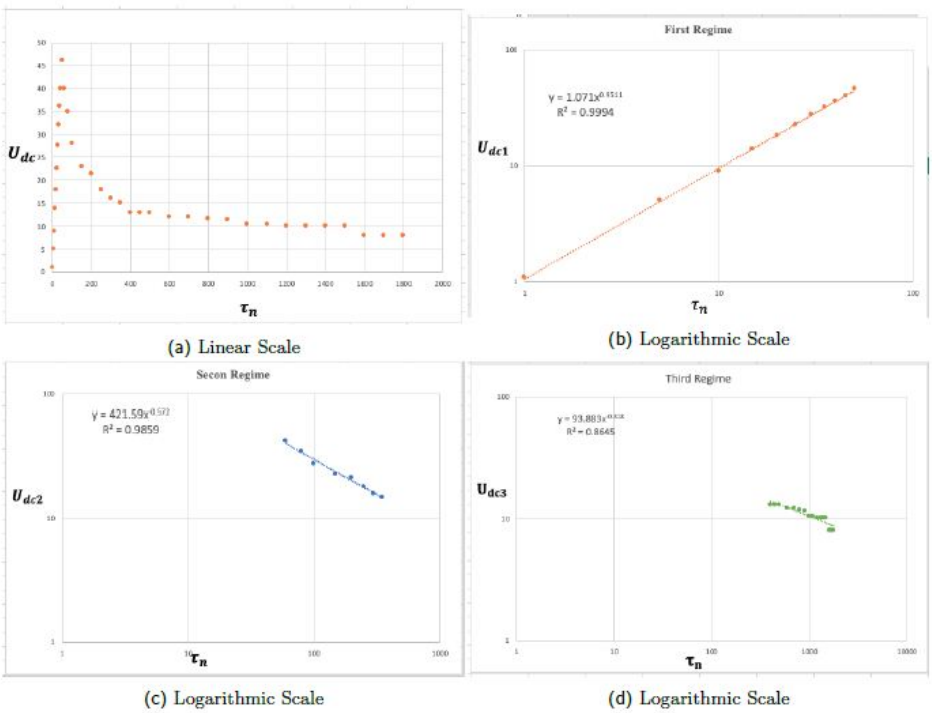

(a) Linear Scale (b) Logarithmic Scale

(c) Logarithmic Scale (d) Logarithmic Scale

Fig. 12. Propagation speed of the Density current U_{dc} for the different Regimes with respect to time τ_n

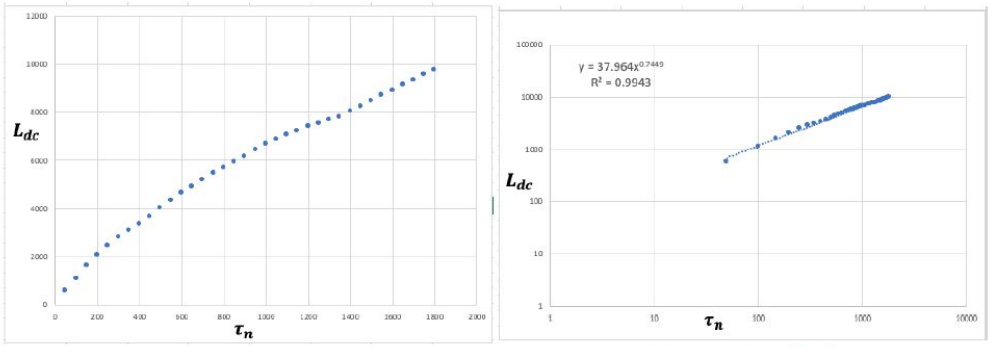

(a) Linear Scale (b) Logarithmic Scale

Fig. 13. Variation of spreading distance of the density current L_{dc} with respect to time τ_n

it in turn overtakes the penetrating head of the current. It was reported earlier that at this point in the flow, the penetrating head advances as $t^{\frac{2}{3}}$, but decreases with front speed as $t^{-\frac{1}{3}}$ [2, 6, 11, 19]. However, the results here appear slightly different in terms of the scaling laws. The rapid depletion of temperature in this case resulted in a very slow advancement of the fluid. Fig. 12(c) explain this fact with a downward slop as temperature in the denser fluid at this point had reduced drastically and not energetic to accelerate faster. Therefore, we can identify a single regime in this phase of flow from an empirically determined data set, and this is

shown as a fairly straight line that represents the best fit power laws obtained by linear regression of $logU_{dc2}$ on $log\tau_n$:

$$U_{dc2} = 421.59\tau_n^{-0.572} \quad [R^2 = 0.9859] \quad (3.2)$$

where R^2 is the regression coefficient in each case.

The third phase is the stepwise movement phase which correspond to the phase where viscous effects overcome inertial effects and the current front velocity decreases more rapidly as $t^{-\frac{4}{5}}$, with front position advancing as $t^{\frac{1}{5}}$ [2, 6, 11, 19]. Whereas, the result here also show a very unique behaviour. This was the region much of the Kelvin-Helmholtz instabilities was observed. Such that the raging columns of these instabilities created some sort of partitions in the denser fluid which might be responsible for the stepwise movement. However, we could identify a single regime in this phase of flow from an empirically determined data set, and this is shown in Figure 12(d) as a fairly straight line that represents the best fit power laws obtained by linear regression of $logU_{dc3}$ on $log\tau_n$:

$$U_{dc3} = 93.883\tau_n^{-0.318} \quad [R^2 = 0.8645] \quad (3.3)$$

where R^2 is the regression coefficient in each case.
The result as presented here (see Fig. 12(a)) with a linear scale is similar to the experimentally studied cases by Bukreev [20] and [21], where the author have considered the speed of the surface current at different barrier position.

Spreading distance L_{dc} of the density current were also considered with a linear and logarithmic scale (see Fig. 13(a) and (b)). These data are empirically determined spread length L_{dc} of the density current, measured from the barrier position to a significant distance and plotted against time τ_n. Both results with the linear and logarithmic scale (Fig. 13(a)) indicate that a single regime could be identified, and shown as a straight line that represents the best fit power laws obtained by linear regression of $logL_{dc}$ on $log\tau_n$:

$$L_{dc} = 37.964\tau_n^{0.7449} \quad [R^2 = 0.9943] \quad (3.4)$$

4 CONCLUSION

The behaviour of warm discharge through lock-exchange was investigated, with the assumption that density was taken as a quadratic function of temperature. The results here also show three regimes of flow as recorded in earlier studies together with the development of Kelvin-Helmholtz instability. The general behaviours here are dependent on lock volume, density difference and Reynolds number as also described by [6]. We noticed that the collapsing velocity of the denser fluid within the first time frame was high, higher than every fluid movement elsewhere. Relations that describes the various regimes of flow as given in equation (13), (14) and (15) were also drawn, and as well as those for the spreading distance L_{dc} of the density current in equation (16). However, there are little variations in the scaling laws as compared to the earlier studied cases [6, 19, 25]. It is believed that the velocity of the gravity current is highly influenced by density difference and lock volume (i.e., velocity increases with increasing density difference for those where density variation is as a result of saltwater and a considerably high lock volume). But for those where density difference is as a result of temperature, we believe that these results are a good starting point to better fathom and as well, gain more insight into such studies. Lastly, the consideration of barrier position is key, being that the lock volume is also believed to be a factor. Thus, we believe also that the two cases as considered here is not enough, and as such, we have considered this as a limitation, and there is the need to carryout another investigation to fathom, if the speed of the current is really dependent on the barrier position. This work as presented here is practical and relevant to many fields of study and also enhances policy making towards the protection of the aquatic ecosystems. Because such discharge or introduction of warm but dense water may definitely give rise to environmental problems; where the sudden increase in the water temperature after discharge/introduction

will lead to ”thermal shock” killing aquatic life that has become acclimatised to living in a stable temperate environment. Researchers can also gain more knowledge in terms of the dynamics of such flows.

COMPETING INTERESTS

Authors have declared that no competing interests exist.

REFERENCES

[1] Simpson JE. Gravity Currents: In the Environment and the Laboratory. UK, Cambridge University Press. 1997;258.

[2] George MA, Kay A. Numerical Simulations of the Cabbeling Phenomenon in Surface Gravity Currents in Cold Fresh Water. Journal of Scientific Research & Reports. 2022;28(1):68-85.

[3] Nogueira HI, Adduce C, Alves E, Franca MJ. Dynamics of the head of gravity currents. Environmental Fluid Mechanics. 2014;14(2):519-40.

[4] Tien NN, Cuong DH, Mau LD, Tung NX, Hung PD. Mechanism of Formation and Estuarine Turbidity Maxima in the Hau River Mouth. Water. 2020;12(9):2547.

[5] Nasrollahpour R, Jamal MH, Ismail Z, Ibrahim Z, Jumain M, Mohd Haniffah MR, Ishak DS. Velocity structure of density currents propagating over rough beds. Water. 2021;13(11):1460.

[6] Yin X, He Y, Lu C, Gao S, Liu Q. Experimental Study on Front Spreading of Lock-Exchange Gravity Current with Long Lock Length. Journal of Engineering Mechanics. 2020 Jan 1;146(1):04019113.

[7] Dai A, Huang YL. Experiments on gravity currents propagating on unbounded uniform slopes. Environmental Fluid Mechanics. 2020 Dec;20(6):1637-62.

[8] Prandtl L. Essentials of fluid dynamics. UK, Blackie Son; 1952.

[9] Benjamin TB. Gravity currents and related phenomena. Journal of fluid mechanics. 1968 Jan;31(2):209-48.

[10] Rottman JW, Simpson JE. Gravity currents produced by instantaneous releases of a heavy fluid in a rectangular channel. Journal of Fluid Mechanics. 1983 Oct;135:95-110.

[11] Maggi MR, Adduce C, Negretti ME. Lock-release gravity currents propagating over roughness elements. Environmental Fluid Mechanics. 2022:1-20.

[12] Pelmard J, Norris S, Friedrich H. Statistical characterisation of turbulence for an unsteady gravity current. Journal of Fluid Mechanics. 2020;901.

[13] Negretti ME, Flòr JB, Hopfinger EJ. Development of gravity currents on rapidly changing slopes. Journal of Fluid Mechanics. 2017 Dec;833:70-97.

[14] Martin A, Negretti ME, Hopfinger EJ. Development of gravity currents on slopes under different interfacial instability conditions. Journal of Fluid Mechanics. 2019 Dec;880:180-208.

[15] Dai A, Huang YL. Boussinesq and non-Boussinesq gravity currents propagating on unbounded uniform slopes in the deceleration phase. Journal of Fluid Mechanics. 2021 Jun;917.

[16] George AM, Kay A. Numerical simulations of a line plume impinging on a ceiling in cold fresh water. International Journal of Heat and Mass Transfer. 2017 May 1;108:1364-73.

[17] George AM, Kay A. Warm discharges in cold fresh water: 2. Numerical simulation of laminar line plumes. Environmental Fluid Mechanics. 2017 Apr;17(2):231-46.
DOI: http://dx.doi.org/10.1007/s10652-016-9468-x.

[18] Huppert HE, Simpson JE. The slumping of gravity currents. Journal of Fluid Mechanics. 1980;99(4):785-99..

[19] Nogueira HI, Adduce C, Alves E, Franca MJ. Analysis of lock-exchange gravity currents over smooth and rough beds. Journal of Hydraulic research. 2013;51(4):417-31.

[20] Bukreev VI. Effect of the nonmonotonic temperature dependence of water density on the decay of an initial density discontinuity. Journal of applied mechanics and technical physics. 2006;47(1):54-60.

[21] Bukreev IV. Effect of the Nonmonotonic Temperature Dependence of Water Density on the Propagation of a Vertical Plante Jet. Journal of Applied Mechanics and Technical Physics. 2006;47 (2):169 - 174.

[22] Moore DR, Weiss NO. Nonlinear penetrative convection. Journal of Fluid Mechanics. 1973 Nov;61(3):553-81.

[23] Oosthuizen PH, Paul JT. A numerical study of the steady state freezing of water in an open rectangular cavity. International Journal of Numerical Methods for Heat Fluid Flow; 1996.

[24] COMSOL Multiphysics Cyclopedia. The Finite Element Method (FEM). Available at: https://www.comsol.com/multiphysics/finite-element-method [Accessed 28 April 2016].

[25] Vardakostas S, Kementsetsidis S, Keramaris E. Saline gravity currents with large density difference with fresh water in a valley of trapezoidal shape. Environmental Sciences Proceedings. 2020;2(1):64.

[26] Adduce C, Sciortino G, Proietti S. Gravity currents produced by lock exchanges: experiments and simulations with a two-layer shallow-water model with entrainment. Journal of Hydraulic Engineering. 2012;138(2):111-21.

Peer-review history:
The peer review history for this paper can be accessed here:
https://www.sdiarticle5.com/review-history/85067